Journal of Advanced Ceramics
2020, **9**(4): 511–516
https://doi.org/10.1007/s40145-020-0384-7

ISSN 2226-4108
CN 10-1154/TQ

Rapid Communication

Enhanced ferroelectricity and magnetism of quenched $(1-x)BiFeO_3$–$xBaTiO_3$ ceramics

Han BAI, Jun LI*, Yang HONG, Zhongxiang ZHOU*

School of Physics, *Harbin Institute of Technology*, *Harbin 150001*, *China*

Received: March 8, 2020; Revised: May 6, 2020; Accepted: May 7, 2020

Abstract: Bismuth ferrite ($BiFeO_3$)-based materials are multiferroic materials widely studied. This study reports that strong ferroelectricity and enhanced magnetic performance are simultaneously obtained in the quenched $(1-x)BiFeO_3$–$xBaTiO_3$ (BFBT100x, x = 0.2 and 0.3) ceramics. Quenching treatment can reduce the amount of defects and Fe^{2+} ions and make the defect dipole in a random state, which is conducive to improving the ferroelectricity and magnetism. Compared with the conventional sintered samples, the quenched ceramics have higher remnant and saturation polarization. As for magnetism, the coercive field (H_c) of the quenched ceramics is smaller and the quenching treatment can increase the maximum magnetization by up to 15%.

Keywords: multiferroics; bismuth ferrite ($BiFeO_3$)-based ceramics; quenching treatment

1 Introduction

Multiferroics, where the ferroelectricity and magnetism coexist, have attracted much attention and the magnetoelectric (ME) coupling effect in multiferroics makes the application more extensive. One application for multiferroics is to be used to the next generation high-speed nonvolatile random-access memory (NVRAM) devices [1–3]. Now research on ME NVRAM devices has achieved some gratifying progress [4,5]. However, the magnetoelectric coupling coefficient of the single-phase multiferroics at room temperature is still not large enough to be practically applied.

Bismuth ferrite ($BiFeO_3$) is currently the most studied room-temperature multiferroic, which exhibits ferroelectricity and G-type antiferromagnetism at room temperature simultaneously [6]. The ferroelectric Curie temperature (T_C) is about 830 ℃ and the antiferromagnetic Nèel temperature (T_N) is about 370 ℃. Although larger remnant polarization (P_r) in $BiFeO_3$ has been reported [7,8], it is usually difficult to prepare bulk single-phase $BiFeO_3$ ceramics with stable and robust ferroelectricity due to the presence of the secondary phase ($Bi_2Fe_4O_9$ and $Bi_{25}FeO_{40}$) and large leakage current (due to the existence of Fe^{2+} and vacancy defects) [9]. Wang *et al*. [10] pioneered the rapid liquid phase sintering method to prepare high resistivity single-phase $BiFeO_3$ ceramics. The rapid liquid phase sintering method avoids the secondary phase by a high rate of heating and cooling (100 ℃/s). Zhang *et al*. [11] developed a simpler and more practical quenching sintering method based on the rapid liquid phase sintering technique, directly quenched the samples from high temperature to room temperature after sintering. The obtained pure $BiFeO_3$ ceramic possessed a well-saturated ferroelectric hysteresis loop and large P_r (11.8 μC/cm^2). Shi *et al*. [12] analyzed the mechanism of the enhanced

* Corresponding authors.
E-mail: J. Li, lijuna@hit.edu.cn;
Z. Zhou, zhouzx@hit.edu.cn

ferroelectricity in the $BiFeO_3$-based single-phase ceramic obtained by the quenching method. In their view, the quenching process can reduce the pinning effect of the defect dipoles on the ferroelectric domain walls, enhancing the mobility of the domain walls and improving its ferroelectric performance. Although robust ferroelectricity can be obtained by the quenching process in $BiFeO_3$, the existence of the antiferromagnetism makes it difficult to exhibit a relatively obvious ME coupling effect, which greatly limits the application of $BiFeO_3$ as a multiferroic material. To improve the application, the usual practice is to make the $BiFeO_3$ and other ABO_3-type ferroelectrics form solid solutions [13–16]. Not only can it improve ferroelectricity, but also destroy the antiferromagnetic structure in $BiFeO_3$ to obtain weak ferromagnetism. Among these solid solutions, $(1–x)BiFeO_3–xBaTiO_3$ (BFBT100x) ceramics are promising multiferroics with good performance. Weak ferromagnetism can appear in BFBT100x ceramics due to that the Ti^{4+} in B-site destroys the antiferromagnetic structure of $BiFeO_3$ [17]. Besides, BFBT100x ceramics usually possess good ferroelectric hysteresis loops with high P_r (20–30 μC/cm^2) [18,19]. Due to the high T_C of $BiFeO_3$ (T_C = 830 ℃), BFBT100x ceramics also have a high T_C. Together with the high piezoelectricity (d_{33} ≈ 400 pC/N) [20] and large strain properties (S = 0.32% and d^*_{33} = 800 pm/V) [21,22], BFBT100x ceramics can be a promising candidate for the high-temperature piezoelectric material.

In this study, we studied the ferroelectricity and magnetism of $(1–x)BiFeO_3–xBaTiO_3$ (x = 0.2 and 0.3) prepared by the conventional sintering method and the quenching method. It was found that robust ferroelectricity and enhanced magnetism were obtained in the quenched samples.

2 Experimental

The multiferroic ceramics $(1–x)BiFeO_3–xBaTiO_3$ (BFBT100x, x = 0.2 and 0.3, abbreviated as BFBT20 and BFBT30, respectively) were prepared using the stating materials of Bi_2O_3 (99.0%), Fe_2O_3 (99.9%), $BaCO_3$ (99.9%), and TiO_2 (99.0%). All powders weighed in stoichiometric ratio were placed into agate milling containers with ethanol and then ball-milled for 8 h at 250 rpm. The dried powder was pressed into disk-shaped samples with a diameter of 30 mm under the pressure of 80 MPa and then calcined at 800 ℃ for 4 h in air atmosphere. The calcined samples were ball-milled again for 8 h. Polyvinyl alcohol (PVA) was added as a binder to the powder. The disk-shaped samples with a thickness of about 1 mm and a diameter of 8 mm can be obtained under the pressure of 400 MPa. Before sintering, the samples were kept at 500 ℃ for 4 h to volatilize the organic binder of PVA. We used two sintering methods. One is the conventional sintering method that is to sintering samples at 1000 ℃ for 4 h at a heating and cooling rate of 5 ℃/min (the samples sintered with this method abbreviated as BFBT20-CS and BFBT30-CS). The other method is the quenching method. The samples were directly put into the tube furnace, which was heated up to 1000 ℃ in advance. After 30 min, the samples were subsequently quenched in water (the samples sintered with this method abbreviated as BFBT20-Q and BFBT30-Q). For electrical measurement, the samples were polished to 0.3 mm in thickness and the Ag electrodes were fired at 800 ℃ for 30 min.

Powder X-ray diffraction (XRD) data was collected by a diffractometer (PANalytical Empyrean) with a Cu Kα radiation tube at 40 kV and 40 mA. The morphology of the samples was examined by scanning electron microscope (SEM, Carl Zeiss Merlin Compact) with a secondary electron mode. The dielectric properties were measured by the LCR analyzer (TH2827). The magnetic hysteresis loops were measured by a vibrating sample magnetometer (VSM, Lake Shore 7410). Ferroelectric hysteresis loops (P–E) were measured using a ferroelectric tester (Radiant Precision Premier II).

3 Results and discussion

The morphology and structure characteristics of BFBT100x ceramics are shown in Fig. 1. Figures 1(a)–1(d) display the fracture surface images of BFBT20-CS, BFBT20-Q, BFBT30-CS, and BFBT30-Q ceramics, respectively. All the ceramics showed very dense grain arrangement and almost no pores. The grains obtained by the conventional sintering method are significantly larger than those by the quenching method. This is due to that grains have enough time (4 h) to grow in the conventional sintering method. Figures 1(e) and 1(f) exhibit the XRD patterns and the enlarged view of peaks near 31.7°. There are no impurity phases in patterns. In the enlarged view, the patterns of two BFBT30 samples only present a single peak. According to Refs. [23,24],

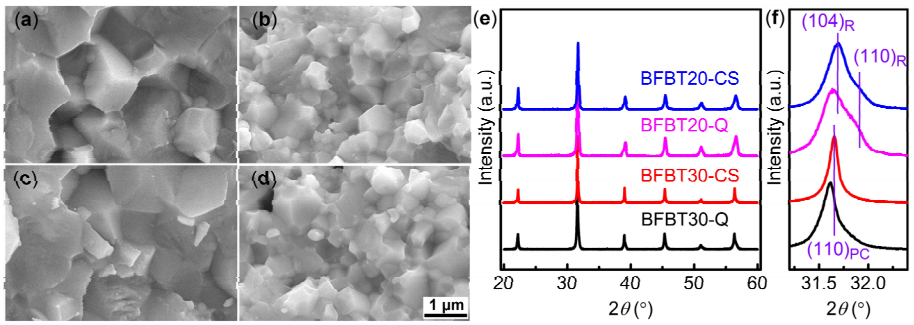

Fig. 1 Morphology and structure properties of BFBT100*x* ceramics. (a–d) Fracture surface images of BFBT20-CS, BFBT20-Q, BFBT30-CS, and BFBT30-Q ceramics, respectively; (e) XRD patterns of four ceramics; (f) the enlarged view of the peaks near 31.7°.

it can conclude that BFBT30-CS and BFBT30-Q samples are pseudo-cubic (PC) structure and the single peak near 31.7° is specified as $(100)_{PC}$ peak. In BFBT20-CS and BFBT20-Q samples, there are two peaks near 31.7° in the XRD patterns, which correspond to $(104)_R$ and $(110)_R$ peaks of the rhombohedral (R) $BiFeO_3$ phase. Since the intensity of $(104)_R$ is closed to that of $(110)_R$ in the $BiFeO_3$ phase, the structure of BFBT20 ceramics should be coexistence of rhombohedral and PC phase (R+PC). Besides, the relative intensity of $(110)_R$ in BFBT20-Q ceramic is slightly higher than that in the BFBT20-CS sample, indicating that the proportion of R phase in R+PC structure is higher in BFBT20-Q ceramic. The width of the peak in the quenched samples are both larger than that in the conventional sintered samples. It is attributed to a smaller grain size in the quenched samples. The short sintering time (30 min) of the quenched samples not only makes the grain size smaller but also reduces the concentration of defects caused by the Bi volatilization. A large concentration of defect will decrease the lattice constant to a certain degree. Hence, in the quenched samples, the position of the diffraction peak moves to a lower angle than that in the conventional sintered samples, which means a higher lattice constant.

The temperature-dependent dielectric constant (ε_r) results are presented in Fig. 2. Obvious ferroelectric phase transition peaks were observed in all samples. All transition peaks present frequency-dependent characteristic, which means the ferroelectric phase transition is a typical relaxation ferroelectric phase transition. This is consistent with the results in Refs. [25,26]. In the BFBT20-CS sample, the dielectric constant continues to rise after the temperature is higher than T_C. This should be attributed to the leakage current excited at high temperatures. Due to the long sintering time of the conventional sintering method, more defects caused by Bi volatilization will be formed, which will cause a large leakage current, but the leakage contribution of the quenched sample (Fig. 2(b)) is quickly suppressed. In BFBT30-CS and BFBT30-Q samples, the dielectric curves are similar, and both show relaxation ferroelectric phase transition curves. The T_C is 386 and 390 ℃ at 1 kHz, respectively. The similar T_C shows that the phase structure of the two samples has not changed significantly, which is similar to the results of

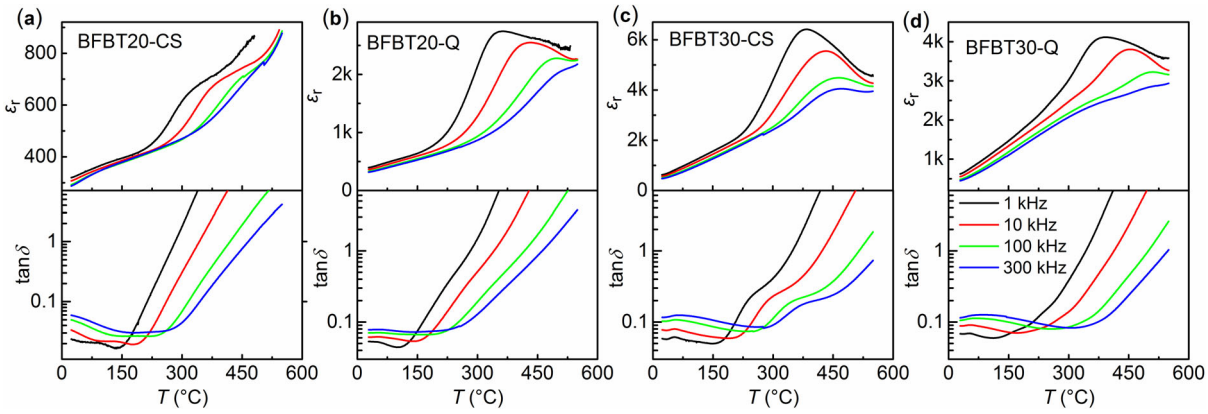

Fig. 2 ε_r and tanδ results of BFBT100*x* ceramics.

the XRD discussion above. The difference between the dielectric curves of the BFBT20-CS and BFBT30-CS samples may come from the difference in the structure of the two components. The loss results are in logarithmic form. From room temperature to about 200–300 ℃, the loss is relatively small and has been maintained less than 0.1. However, as temperature increases, the loss increases rapidly in all samples, which is attributed to an interfacial polarization mechanism.

Figures 3(a)–3(d) present the ferroelectric hysteresis loops under different excitation electric fields (E) at 10 Hz of ceramics. The hysteresis loop of BFBT20-CS ceramic is shown in Fig. 3(a). The hysteresis loops under different external field excitations are close to a straight line, which means that there is only dielectric contribution without any ferroelectric contribution. Besides, when E exceeding 60 kV/cm is applied, the BFBT20-CS ceramic will be broken down. However, the BFBT20-Q ceramic shows typical and saturated ferroelectric hysteresis loops (Fig. 3(b)). A complete hysteresis loop can still be obtained on BFBT20-Q ceramics when the excitation E reaches 90 kV/cm and the P_r can reach 18.2 μC/cm^2. This difference in ferroelectricity also appears in BFBT30 ceramics. The ferroelectric hysteresis loops of BFBT30-CS ceramic (Fig. 3(c)) shows a certain ferroelectric contribution, but it is difficult to reach saturation. The maximum E it can bear is 70 kV/cm. However, similar to the hysteresis loop of the BFBT20-Q sample, the quenched BFBT30-Q ceramic exhibits typical saturated hysteresis loops and the P_r is 17.6 μC/cm^2 (E = 90 kV/cm). The ferroelectricity of the above BFBT100x ceramics demonstrates the importance of sintering method. During the high-temperature sintering process, the Bi element volatilizes in the form of Bi_2O_3 [22], which will form Bi vacancies. To achieve electrical neutrality, oxygen vacancies and divalent irons (Fe^{2+}) will be bound to occur. These defects will form defect dipoles. In the conventional sintering process, a long time (4 h) sintering process will produce enough defects, which will form many defect dipoles. The defect dipoles will align themselves in the polarization direction within domains during the long cooling process. The arranged defect dipoles can greatly hinder the movement of the domain walls, which will greatly reduce the ferroelectricity [27]. On the other hand, more Fe^{2+} ions can also reduce the ferroelectricity to a certain extent and reduce the electrical insulating property of ceramics [28]. These are the reasons for the poor ferroelectricity and low electrical breakdown strength of the BFBT20-CS and FBT30-CS ceramics. While in the quenching sintering process, short sintering time will reduce the formation of defects and the number of defect dipoles will also decrease. The quenching process can reduce the temperature of the ceramic to room temperature in a few seconds and the defect dipoles will align randomly. This can make the domain walls be more mobile and generate better ferroelectricity with larger P_r. For the enhanced ferroelectricity of BFBT20-Q ceramic, in addition to the above reasons, it is also related to the phase structure. As discussed above, the proportion of the R phase is higher in the R+PC structure of BFBT20-Q ceramic. This is also considered to be a reason for the ferroelectricity enhancement of this ceramic.

The magnetic hysteresis loops of ceramics with a magnetic field (H) range of (−15)–15 kOe measured

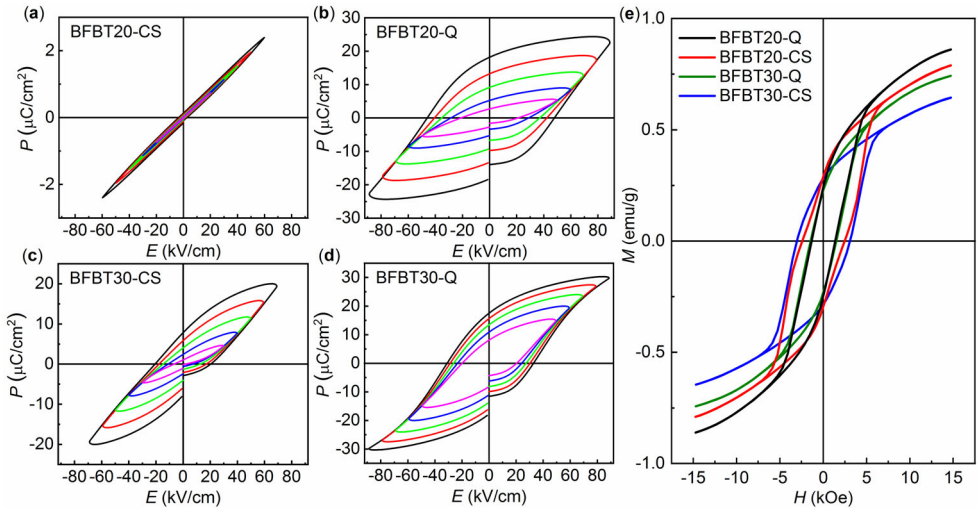

Fig. 3 (a–d) Ferroelectric hysteresis loops measured at10 Hz and (e) magnetic hysteresis loops measured at room temperature.

at room temperature are displayed in Fig. 3(e). Ti ions in BFBT100*x* ceramics occupy the B-site, destroying the antiferromagnetic structure of the modulated spiral spin of $BiFeO_3$, so all samples present weak ferromagnetism. The remnant magnetizations of the four samples are all about 0.26 emu/g, which is similar to the values in Refs. [29,30]. The maximum magnetization (M_{max}) is 0.79 and 0.64 emu/g for BFBT20-CS and BFBT30-CS samples, respectively. For BFBT20-Q and BFBT30-Q samples, the M_{max} rises to 0.86 and 0.74 emu/g, respectively. The quenching treatment can increase the M_{max} of BFBT20 and BFBT30 samples by 9% and 15%, respectively. This is due to the decrease in the amount of Fe^{2+} ions produced by Bi volatilization in the quenched sample. Moreover, the magnetic coercive force (H_c) is significantly reduced in quenched samples. In the quenched process, short sintering time and a very fast cooling rate can produce fewer defects and defect dipoles. The arrangement of defective dipoles is more random. The resistance to the movement of the domain walls will become smaller, which will lead to a small H_c. Therefore, the quenching treatment can increase the magnetization and reduce the coercivity force to some extent.

4 Conclusions

The ferroelectric and magnetism were investigated in the BFBT20 and BFBT30 samples obtained by two sintering methods: conventional sintering method and quenching sintering process. Quenched samples have smaller grain size than conventional sintered ceramics due to short sintering time. The reduction of the defect concentration caused by the volatilization of Bi in the quenched sample will make the lattice constant larger, which is shown in the XRD patterns as the peak moves to a lower angle. The high-temperature leakage current contribution of the loss curve is suppressed in quenched ceramics. The quenching treatment can greatly improve the ferroelectricity of ceramics and both the quenched samples show saturated ferroelectric hysteresis loops. For magnetic properties, the coercive field of the quenched sample is smaller and the quenching treatment can increase M_{max} by up to 15% in BFBT30 ceramics.

Acknowledgements

This study was supported by the National Natural Science Foundation of China (51502054), the Postdoctoral Science Foundation of China (2014M551236), and the Postdoctoral Science Foundation of Heilongjiang Province (LBH-Z14083).

References

[1] Eerenstein W, Mathur ND, Scott JF. Multiferroic and magnetoelectric materials. *Nature* 2006, **442**: 759–765.

[2] Gajek M, Bibes M, Fusil S, *et al*. Tunnel junctions with multiferroic barriers. *Nat Mater* 2007, **6**: 296–302.

[3] Shen JX, Cong JZ, Chai YS, *et al*. Nonvolatile memory based on nonlinear magnetoelectric effects. *Phys Rev Applied* 2016, **6**: 021001.

[4] Scott JF. Multiferroic memories. *Nat Mater* 2007, **6**: 256–257.

[5] Bibes M, Barthélémy A. Towards a magnetoelectric memory. *Nat Mater* 2008, **7**: 425–426.

[6] Sosnowska I, Neumaier TP, Steichele E. Spiral magnetic ordering in bismuth ferrite. *J Phys C*: *Solid State Phys* 1982, **15**: 4835–4846.

[7] Neaton JB, Ederer C, Waghmare UV, *et al*. First-principles study of spontaneous polarization in multiferroic $BiFeO_3$. *Phys Rev B* 2005, **71**: 014113.

[8] Choi T, Lee S, Choi YJ, *et al*. Switchable ferroelectric diode and photovoltaic effect in $BiFeO_3$. *Science* 2009, **324**: 63–66.

[9] Wu JG, Fan Z, Xiao DQ, *et al*. Multiferroic bismuth ferrite-based materials for multifunctional applications: Ceramic bulks, thin films and nanostructures. *Prog Mater Sci* 2016, **84**: 335–402.

[10] Wang YP, Zhou L, Zhang MF, *et al*. Room-temperature saturated ferroelectric polarization in $BiFeO_3$ ceramics synthesized by rapid liquid phase sintering. *Appl Phys Lett* 2004, **84**: 1731–1733.

[11] Zhang ST, Lu MH, Wu D, *et al*. Larger polarization and weak ferromagnetism in quenched $BiFeO_3$ ceramics with a distorted rhombohedral crystal structure. *Appl Phys Lett* 2005, **87**: 262907.

[12] Shi XX, Qin Y, Chen XM. Enhanced ferroelectric properties in $Bi_{0.86}Sm_{0.14}FeO_3$-based ceramics. *Appl Phys Lett* 2014, **105**: 192902.

[13] Freitas VF, Dias GS, Protzek OA, *et al*. Structural phase relations in perovskite-structured $BiFeO_3$-based multiferroic compounds. *J Adv Ceram* 2013, **2**: 103–111.

[14] Zheng T, Wu JG. Enhanced piezoelectric activity in high-temperature $Bi_{1-x-y}Sm_xLa_yFeO_3$ lead-free ceramics. *J Mater Chem C* 2015, **3**: 3684–3693.

[15] Lv J, Wu JG, Wu WJ. Enhanced electrical properties of quenched $(1-x)Bi_{1-y}Sm_yFeO_3$–$xBiScO_3$ lead-free ceramics. *J Phys Chem C* 2015, **119**: 21105–21115.

[16] Hang QM, Zhou WK, Zhu XH, *et al*. Structural, spectroscopic, and dielectric characterizations of Mn-doped $0.67BiFeO_3$–$0.33BaTiO_3$ multiferroic ceramics. *J Adv Ceram* 2013, **2**: 252–259.

[17] Kumar MM, Srinath S, Kumar GS, *et al*. Spontaneous magnetic moment in $BiFeO_3$–$BaTiO_3$ solid solutions at low temperatures. *J Magn Magn Mater* 1998, **188**: 203–212.

[18] Zheng T, Jiang ZG, Wu JG. Enhanced piezoelectricity in $(1-x)Bi_{1.05}Fe_{1-y}A_yO_3$–$xBaTiO_3$ lead-free ceramics: site engineering and wide phase boundary region. *Dalton Trans* 2016, **45**: 11277–11285.

[19] Zheng T, Ding Y, Wu JG. Bi nonstoichiometry and composition engineering in $(1-x)Bi_{1+y}FeO_{3+3y/2}$–$xBaTiO_3$ ceramics. *RSC Adv* 2016, **6**: 90831–90839.

[20] Lee MH, Kim DJ, Park JS, *et al*. High-performance lead-free piezoceramics with high curie temperatures. *Adv Mater* 2015, **27**: 6976–6982.

[21] Zheng T, Zhao CL, Wu JG, *et al*. Large strain of lead-free bismuth ferrite ternary ceramics at elevated temperature. *Scripta Mater* 2018, **155**: 11–15.

[22] Zhu LF, Liu Q, Zhang BP, *et al*. Temperature independence of piezoelectric properties for high-performance $BiFeO_3$–$BaTiO_3$ lead-free piezoelectric ceramics up to 300 ℃. *RSC Adv* 2018, **8**: 35794–35801.

[23] Li Q, Wei JX, Cheng JR, *et al*. High temperature dielectric, ferroelectric and piezoelectric properties of Mn-modified $BiFeO_3$–$BaTiO_3$ lead-free ceramics. *J Mater Sci* 2017, **52**: 229–237.

[24] Gao WW, Lv J, Lou XJ. Large electric-field-induced strain and enhanced piezoelectric constant in CuO-modified $BiFeO_3$–$BaTiO_3$ ceramics. *J Am Ceram Soc* 2018, **101**: 3383–3392.

[25] Zheng DG, Zuo RZ. Enhanced energy storage properties in $La(Mg_{1/2}Ti_{1/2})O_3$-modified $BiFeO_3$–$BaTiO_3$ lead-free relaxor ferroelectric ceramics within a wide temperature range. *J Eur Ceram Soc* 2017, **37**: 413–418.

[26] Liu J, Liu XQ, Chen XM. Ferroelectric and magnetic properties in $(1-x)BiFeO_3$–$x(0.5CaTiO_3$–$0.5SmFeO_3)$ ceramics. *J Am Ceram Soc* 2017, **100**: 4045–4057.

[27] Kim DS, Cheon CI, Lee SS, *et al*. Effect of cooling rate on phase transitions and ferroelectric properties in $0.75BiFeO_3$–$0.25BaTiO_3$ ceramics. *Appl Phys Lett* 2016, **109**: 202902.

[28] Lv J, Lou XJ, Wu JG. Defect dipole-induced poling characteristics and ferroelectricity of quenched bismuth ferrite-based ceramics. *J Mater Chem C* 2016, **4**: 6140–6151.

[29] Park TJ, Papaefthymiou GC, Viescas AJ, *et al*. Composition-dependent magnetic properties of $BiFeO_3$–$BaTiO_3$ solid solution nanostructures. *Phys Rev B* 2010, **82**: 024431.

[30] Cheng S, Zhang BP, Zhao L, *et al*. Enhanced insulating and piezoelectric properties of $0.7BiFeO_3$–$0.3BaTiO_3$ lead-free ceramics by optimizing calcination temperature: analysis of Bi^{3+} volatilization and phase structures. *J Mater Chem C* 2018, **6**: 3982–3989.